SDC-92-186

SDC
SOLENOIDAL DETECTOR NOTES

RADIATION HARDNESS STUDY OF SCINTILLATING TILE/FIBERS

March 19, 1992

K. Hara, H. Hirade, T. Iinuma, T. Kaneko, S. Kim, Y. Miyamoto, I. Nakano, M. Okabe, J. Suzuki, H. Takahashi, K. Takikawa and K. Yasuoka
Univeristy of Tsukuba

SDC-92-00186
CDF-1679
UTPP-41
March 19, 1992

Radiation Hardness Study of Scintillating Tile/Fibers

K. Hara, H. Hirade, T. Iinuma, T. Kaneko, S. Kim, Y. Miyamoto, I. Nakano,
M. Okabe, J. Suzuki, H. Takahashi, K. Takikawa, and K. Yasuoka

Institute of Physics, University of Tsukuba
Tsukuba, Ibaraki 305, Japan

Abstract

We have investigated the ^{60}Co-induced damage of scintillating tile/fibers. Additional radiation-induced nonuniformity is observed above 1 Mrad. However, the changes are less than $\pm 1\%$ below 0.6 Mrad without respect to the dose imbalance in a tile. Dose rate dependence of the radiation damage is very weak in the range 6-360 krad/h. No significant improvement in radiation hardness is obtained in the samples irradiated in nitrogen and annealed in air. The damage induced by 2.5-GeV electron showers is in agreement with the ^{60}Co-induced damage. Our results on the radiation hardness are independent of how to evaluate it by ^{106}Ru-induced current, penetrating β rays, or high energy electron beam. The radiation hardness of the tile/fibers using a green tile with an orange fiber is better than those using a blue tile with a green fiber, although the relative light yield of the latter is better than the former due to less sensitivity of the photomultiplier to orange lights. Especially the 3HF/O2 is significantly radiation-resistant. In comparison between the SCSN81/Y7 and SCSN81/BCF91A, no significant difference is observed in the relative light yield and the radiation hardness.

1 Introduction

Recently radiation hardness tests of tile/fiber electromagnetic calorimeter test modules have been made with several GeV electrons at several sites; Beijing [1], KEK [2], and Saclay [3]. In our studies at KEK, we reported that 2.5-GeV electron induced damage in the test module, which was irradiated to 0.6-Mrad at the shower peak, showed effects of 28% light loss at the shower maximum layer and 19% loss in the total pulse height for 2-GeV electrons. Meanwhile, in the last few years, many groups have been studying radiation damage of scintillators using relatively low energy electrons and ^{60}Co γ-rays [4]. Are these damages the same as the high energy electron induced ones ?

At the SSC, minimum bias π^0's mainly contribute to the dose deposition and their transverse momentum is 0.6 GeV/c on the average. Low-energy electrons and photons developed in an electromagnetic shower have some possibility of destroying scintillating dyes and base materials, polystyrene and PMMA, and of producing radicals in these base materials. One could imagine that the destruction of dyes directly affects to the radiation damage and makes degradation of light yields. In a real scintillator, however, the destruction of dyes is somewhat insensitive to degradation of light yields since concentration of dyes is optimized to cause saturation in light yields. On the other hand, the production of radicals in base materials makes color centers [4][5], resulting in degradation of light transmission. After heavy irradiation, plastic scintillators at least made of polystyrene and PMMA get darken and yellow. In general, short-wavelength lights are more absorbable than long-wavelength lights in these materials. Therefore, a green scintillator is expected to be harder against radiation than a blue one.

Once the small molecules of scintillating dyes are destroyed, their restoration is not much expected. Meanwhile, radicals created in polymers of a base material have chances of recombining. If color centers vanish, the light transmission would be cleared to scintillating lights and annealed. The process of recombination and its chances might be dependent on irradiation conditions, e.g. dose rates and gas environment [5]. Detailed mechanism in producing and annealing of color centers is not well known yet.

Since it is hard to make radiation damage studies under the same conditions as expected at the SSC, we are obliged to make acceleration tests. Even in the acceleration test, the irradiation conditions have to be maintained similar as much as possible to those expected at the SSC.

A dose rate usually means an instantaneous one defined by taking the ratio of a total dose to an irradiation time. At the SSC, the maximum radiation dose that occurs at electromagnetic shower maximum is estimated [6] to be 58 krad at pseudorapidity $\eta = 1.5$ and 5.7 Mrad at $\eta = 3$ for 10 years of operation at the design luminosity of 10^{33} cm^{-2}sec^{-1}. The corresponding instantaneous dose rate is 2 rad/h at $\eta = 1.5$ and 200 rad/h at $\eta = 3$, respectively. These numbers were estimated by assuming an effective operation time of 10^7 sec in a year. The remaining time due to loss time between beam injections would be spent without any irradiations. Therefore, another definition might be also useful to describe the effects of dose rates on the radiation damage. That is an averaged dose rate defined by taking the ratio of a total dose to elapsed time (irradiation time plus annealing time) in exposure.

Since a ^{60}Co exposure study is relatively easier than a study using several-GeV electron beam, comparison of ^{60}Co-induced damage and beam induced damage is essential in planning future radiation hardness tests. In this report, we compare ^{60}Co-induced damage with 2.5-GeV electron-induced damage. We evaluate the damage in three different ways.

In Section 2, we describe the samples of scintillating tiles and waveshifting fibers used in this study. A splicing method is presented there. In Section 3, we present how to measure light yields of scintillating tile/fiber and how to evaluate radiation damage. We also mention how to measure radiation doses in irradiation. In Section 4, we describe annealing of radiation damage observed right after irradiation, and permanent damage. Since scintillating tile/fibers placed at large pseudorapidity at the SSC are subject to nonuniform irradiation in a tile, we investigate radiation-induced nonuniformity in Section 5. The dose rate dependence is one of the most important issues in discussing the radiation hardness of scintillators. We present it in Section 6. There are reports indicating effects of gas environments on the radiation damage and its annealing [4],[7]. We investigate the effects and compare the radiation damage between samples irradiated in nitrogen and in air. In Section 7, we compare the radiation hardness among several different kinds of tile/fibers. We also compare the results observed under continuous irradiation condition and discontinuous irradiation condition that may explicitly allow annealing of the radiation damage.

2 Scintillating Tile and Waveshifting Fiber

Figure 1 shows a scintillating tile used in this study. The scintillating tile is an 11.1 cm $\times$ 11.1 cm wide and 0.3 cm thick polystyrene-based plastic scintillator. The tile has a tiny cut of 0.3 cm $\times$ 3.0 cm to extract a fiber outside. A U-shaped groove is 1.1 mm wide and 1.1 mm deep. The tile edge and groove were machined with an NC cutter. The tile edge was optically polished by hand, while the groove surface was not polished.

The waveshifting fiber is 1 mm in diameter and 50 to 100 cm long. The clear fiber is also 1 mm in diameter and 10 to 50 cm long.

The samples were Kuraray SCSN38, SCSN81, SCSN81Y7, and 3HF scintillating tiles, and Kuraray Y7, O2, and Bicron BCF91A waveshifting fibers. Concentration of waveshifting dyes was optimized to 150 ppm for the Y7 and 100 ppm for the O2. The other dye concentrations were standard.

A scintillating tile/fiber was assembled by embedding a waveshifting fiber in the U-shaped groove. Part of waveshifting fiber inside a tile was 30-cm long. The tile was wrapped in a piece of white paper to increase light yields by a factor of 1.5 and to achieve better response uniformity. Table 1 shows a list of samples used in this study. The samples of group number 1-6 were irradiated with 2.5-GeV electron beams [2] and those of group number 7-14 with ^{60}Co sources.

The Y7 fibers used in calorimeter test modules (Group name A-C) were spliced to clear fibers with a heat-welding method[10]. In our case[11], a waveshifting fiber and a clear fiber

Table 1: List of samples used in this radiation hardness test.

Group#	No. of T/F's	Sample	Exposure	Env. (irr./ann.)	Dose (Mrad)	Evaluation	
						Dosimeter	Light Yield
1 (A)	–	81/Y7	2.5-GeV e^-	air/air	0.8	RCD/CTA	2-GeV e^-
2 (B)	9	81/Y7	2.5-GeV e^-	air/air	0.4	RCD/CTA	2-GeV e^-, Ru-I
3 (C)	9	81/Y7	2.5-GeV e^-	air/air	5.0	RCD/CTA	Ru-I
4 (E_1)	11	81/Y7	2.5-GeV e^-	air/air	0.5	RCD	Ru-I
5 (E_2)	11	81/Y7	2.5-GeV e^-	air/air	1.1	RCD	Ru-I, Sr-$N_{p.e.}$
6 (E_3)	11	81/Y7	2.5-GeV e^-	N_2/air	1.1	RCD	Ru-I
7 (G)	8	81/Y7	^{60}Co γ	air/air	1.2	RCD	Ru-I
8 (G)	8	81/Y7	^{60}Co γ	air/air	9.3	RCD	Ru-I
9 (H)	1	81/Y7	^{60}Co γ	air/air	1.1	RCD	Ru-I
10 (H)	1	81/Y7	^{60}Co γ	air/air	0.035	RCD	Ru-I
11 (I)	3	81/Y7	^{60}Co γ	air/air	0.62	RCD	Ru-I
12 (I)	2	81/Y7	^{60}Co γ	air/air	0.62	RCD	Sr-$N_{p.e.}$
13 (J)	2	81/Y7	^{60}Co γ	air/air	0.43	RCD	Ru-I
14 (J)	2	81/Y7	^{60}Co γ	air/air	1.1	RCD	Ru-I
15 (K)	8	81/Y7	^{60}Co γ	air/air	6.9	RCD	Ru-I
16 (L)	8	81/Y7	^{60}Co γ	air/air	7.1	RCD	Ru-I
17 (L)	8	81/BCF	^{60}Co γ	air/air	7.1	RCD	Ru-I
18 (L)	8	38/Y7	^{60}Co γ	air/air	7.1	RCD	Ru-I
19 (L)	8	81Y7/O2	^{60}Co γ	air/air	7.1	RCD	Ru-I
20 (L)	8	3HF/O2	^{60}Co γ	air/air	7.1	RCD	Ru-I

Notes::

Ru-I : ^{106}Ru-induced currents.

Sr-$N_{p.e.}$: Number of photoelectrons measured with ^{90}Sr.

(irr./ann.) : (gas environment in irradiation / in annealing).

CTA: Cellulose Triacetate Film [8].

RCD: Radiachromics Film [9].

were inserted into 2 cm-long glass tube. The glass tube was 1.1 mm in inner diameter and 0.25 mm thick. While pushed by hands, the fibers were heated at the center of the tube coiled with a 3.5 Ω Nichrome wire, to which a direct current of 0.6 A was supplied by a DC power supply through a 0.5 Ω external resistor. The supplied current was controlled by a timer box consisting of several switch elements. The best heat-welding condition was determined by changing an initial time duration to heat up fibers and the next time duration to keep a temperature stable by switching on and off the current. Light loss was evaluated by using a re-spliced Y7 fiber of two 50-cm long fibers, which were originally a 100-cm long Y7 fiber, and by measuring a light yield drop at the splicing point. The best light transmission was achieved at the initial time duration of 2.5 sec and the total heating time of 20 sec. This method can provide us with $90 \pm 5\%$ transmission at the splicing point.

3 Evaluation of Light Yield and Dose

Figure 2 shows a schematic view of 2-dimensional scanner used in ^{106}Ru-induced current measurements. A sample tile/fiber was set up together with a reference tile/fiber in a light-shielding box made of 1-mm thick aluminum. The fibers from both the sample and the reference tiles were coupled to a 3-cm square and 7.5-cm long light mixer and viewed by a photomultiplier, Hamamatsu R580, operated at -1.0 kV. The light mixer makes a photomultiplier response insensitive to lateral fiber positions.

The ^{106}Ru source was 2-dimensionally scanned in 2 mm steps from the outside of the light shielding box. The ^{106}Ru-induced current from a scintillating tile/fiber was measured with a picoammeter, Keithley 485. After scanning, the source was moved to the center of the reference tile again so as to investigate photomultiplier gain variation during the measurement. From a comparison of the induced currents of the reference tile/fiber measured before and after a sample measurement, we found the photomultiplier gain stability to be within 1 % during the measurement. Photomultiplier dark currents were measured and subtracted from the current readout.

Averaging the currents over 11 points at each central area of both the sample and reference tiles, we evaluated the light yield of each sample. An effective light yield was defined by taking a ratio of the sample light yield to the reference one. The effective light yield thus determined was insensitive to long-term gain variation of the photomultiplier. The actual measuring time was around 5 minutes for a single tile/fiber. Radiation hardness of each sample was defined by taking a ratio of the effective light yield measured after irradiation to that measured before.

In this study, the radiation hardness of most of the samples was evaluated by measuring ^{106}Ru-induced currents. In addition to the induced-current measurement, we investigated another method of photoelectron counting and compared the results for several samples. The number of photoelectrons were evaluated by observing a pulse height distribution with a ^{90}Sr source. Beta rays from the source were collimated with two 5-mm thick lead collimators, which had holes of 2 mm in diameter, and triggered with a 2-mm square scintillation counter viewed

by two photomultipliers, Hamamatsu R329. A scintillating tile/fiber was sandwiched between the two collimators and viewed by a single-photon sensitive photomultiplier, Hamamatsu R464. The pulse height distribution was taken with a CAMAC ADC module, LeCroy 2249A, and fitted to a convolution of a Poisson distribution describing statistics of photoelectron emission and a Gaussian distribution describing fluctuation in electron multiplication. Figure 3 shows pulse height distributions measured before and after ^{60}Co irradiation for the sample I4.

Correlation between ^{106}Ru-induced currents and the number of photoelectrons is shown in Figure 4(a). As expected, strong correlation is observed between these measurements. Figure 4(b) shows a comparison of the radiation damage evaluated by measuring the number of photoelectrons using penetrating electrons and by measuring the ^{106}Ru-induced current. These two measurements of damage are consistent within the measurement error including a systematic error of 4 %.

Irradiation doses are estimated by measuring optical density of Radiachromics film (RCD) [9] at specific wavelengths, 510 and 600 nm. The RCD is a 1 cm x 1 cm and 50-μm thick transparent film. The RCD films were calibrated with a 2-MeV electron beam at Japan Atomic Energy Research Institute at Takasaki. The calibration curve is insensitive to radiation dose rate. At least two films were attached on each group of tile/fibers placed at the same distance from the ^{60}Co source. In the case of nonuniform irradiation for the samples I1-I3, 21 pieces of the RCD films were attached on each tile/fiber so as to measure position dependence of irradiation doses.

4 Annealing and Permanent Damage

Figure 5 shows a schematic view of the setup used for measurements of annealing effects of radiation damage. The sample tile/fiber H1 (H2) was set at a distance of 50 cm from the ^{60}Co source. The reference scintillating tile/fiber was set behind a 24.4-cm thick lead absorber. In order to measure the light yields, the sample and reference tiles were excited with 100 μCi ^{106}Ru sources and viewed by two separate photomultipliers. The ^{106}Ru-induced currents were measured with two picoammeters, Keithley 485.

Before irradiation, initial currents were measured at an operation voltage of -1.0 kV for one hour. Then the samples H1 (H2) was irradiated periodically at a dose rate of 267 krad/h (18 krad/h). The irradiation was interrupted at total doses of 200, 400, 790, and 1100 krad for the sample H1, and at 18 and 45 krad for the H2. Photomultiplier high voltages were turned off during the irradiation. After stopping each irradiation, the current measurement was immediately started at the normal operation voltage. During the total irradiation time of 72 (24) hours, H1 (H2) was kept untouched without any access and the annealing effect of radiation damage was kept track of.

Figure 6 shows a history of radiation damage of the samples H1 and H2. The sample H1 irradiated at an instantaneous dose rate of 264 krad/h clearly shows annealing of the radiation damage with a time constant of 1-4 hours, while the H2 irradiated at a lower dose rate of 18 krad/h does not show a drastic change. The induced currents of H2 and the reference decrease

Table 2: Time constants in annealing and permanent radiation damage

Sample	Exp. Cycle	Dose (krad)	Annealing Time τ(hour)	Current at $\tau \rightarrow \infty$(nA)	Current (Ref.) (nA)	Permanent Damage
H1	Before	0	——	38.71 ± 0.02	35.14 ± 0.02	1.00
	1st	200	3.89 ± 0.13	31.05 ± 0.01	34.60 ± 0.01	0.802 ± 0.001
	2nd	400	0.77 ± 0.12	28.17 ± 0.06	34.19 ± 0.01	0.728 ± 0.002
	3rd	790	3.68 ± 0.04	25.57 ± 0.01	33.82 ± 0.01	0.661 ± 0.001
	4th	1100	2.09 ± 0.02	23.59 ± 0.01	33.51 ± 0.01	0.609 ± 0.001
H2	Before	0	——	34.04 ± 0.03	33.89 ± 0.03	1.00
	1st	18	——	32.30 ± 0.01	33.62 ± 0.01	0.949 ± 0.002
	2nd	45	——	31.06 ± 0.01	33.44 ± 0.01	0.913 ± 0.002

Sample	Time (hour)		Dose Rate (krad/h)		Dose
	Irrad.	Elapsed	Instantaneous	Averaged	(krad)
H1	4.17	46.3	264	23.8	1100
H2	2.5	6.3	18	7.1	45

for several hours due to non-stability of photomultiplier gains and then they get stable. Taking a ratio of the sample current to the reference current, we can cancel or reduce considerable part of variations originating from common sources; e.g. high voltage variation, temperature variation, and so on. Figure 7 shows the ratio of the sample current to the reference current. The ratio is normalized at the start time of the current measurement. The annealing time constants and the final permanent damage were obtained by fitting the annealing curve to an exponential function. The fitted curves are also shown in Figure 6(a). The obtained time constants and permanent damage are summarized in Table 2. The variation of the time constants may be due to various irradiation conditions, e.g. different irradiation time and different annealing time, at a high dose rate.

At a high dose rate, supply of oxygen gas from air would be poor during irradiation. This would take place if the rate of oxygen consumption in a material is greater than the rate at which oxygen can be resupplied by diffusion processes from the surrounding air environment [12]. Thus, the irradiation at the high dose rate resulted in heavier initial damage, which would be strongly dependent on the dose rate and the irradiation time. However, the damage anneals with a time constant of 1-4 hours. The discreapancy between data and the fit at the beginning of annealing in the 3rd irradiation for H1 might be due to restarting of the irradiation before annealing is complete.

5 Uniformity

We investigated radiation-induced change in response uniformity of SCSN81/Y7 tile/fibers irradiated at dose rates of 0.02-0.44 Mrad/h up to doses of 0.35-7.2 Mrad. Two types of nonuniform irradiation were performed by absorbing ^{60}Co γ-rays with iron absorbers, a ring type and a wedge type.

First, nonuniform irradiation with the ring type absorbers was performed to obtain a correction factor to the 2.5-GeV electron-induced damage [2]. The absorbers provided four-step dose variations from the maximum dose at the tile center to the minimum dose at the tile edge. Three tile/fibers, I1-I3, were nonuniformly irradiated at 0.24 Mrad/h with a total of 0.62 Mrad at the center in such a way that the tile edges had three quarters, one half, and one quarter of the center dose. Figure 8 shows response uniformity of the sample irradiated with 67% dose imbalance. Light yields at various points are normalized at a tile center. No significant change in the response map was observed.

Second, the wedge type absorbers were used to simulate nonuniform irradiation expected for tile/fibers at large pseudorapidity in the SSC experiment. According to the evaluation of calorimeter radiation levels at cascade maxima at the SSC [6], dose imbalance is expected to be 0-12%, 13%, 25%, and 44% in a single tile/fiber placed in the barrel region $0 \leq \eta \leq 1.4$ ($\Delta\eta = 0.05$), and in the three endcap regions, $1.4 \leq \eta \leq 1.8$ ($\Delta\eta = 0.05$), $1.8 \leq \eta \leq 2.6$ ($\Delta\eta = 0.1$), and $2.6 \leq \eta \leq 3.0$ ($\Delta\eta = 0.2$), respectively. Here, we performed nonuniform irradiation with 15%, 25%, and 50% dose imbalances at peak-to-peak. Since the tile/fiber used in this study is symmetrical as shown in Figure 1, there are topologically three different types of nonuniform irradiation in respect to the relation between the direction of fiber extraction (a symmetrical axis on a tile/fiber) and the direction of dose-increasing; (A) the symmetrical axis perpendicular to the dose-increasing axis, (B) the symmetrical axis parallel to the dose-increasing axis, and (C) the symmetrical axis anti-parallel to the dose-increasing axis.

Figure 9 shows response uniformity of SCSN81/Y7 tile/fibers exposed under uniform irradiation conditions at 0.69, 1.3, 3.8, and 7.2 Mrad, together with response uniformity measured before irradiation. Figure 10 shows response uniformity of the tile/fibers exposed up to 4.2 Mrad with 25% dose imbalance. The response uniformity was obtained by scanning the ^{106}Ru-source twice, before and after irradiation, to the direction parallel to the symmetrical axis at the tile/fiber center across a waveshifting fiber Y7 at X = −45 mm in Figure 9(a) and to the direction perpendicular to the symmetrical axis at the tile/fiber center across a waveshifting fiber Y7 at Y = ±45 mm in Figures 9(b) and 10. The light yield at each point was normalized using 11 data points at the tile center. The measurement of the radiation induced nonuniformity was performed one week after irradiation. The top, middle, and bottom plots in Figure 10 correspond to three cases described above; (A), (B), and (C). The irradiation dose increases linearly as the scanning point moves to the positive position in the top figure, while it remains constant in the other middle and bottom figures. Radiation induced change in response uniformity is clearly seen around X = ±45 mm and Y = ±35 mm, ±45 mm above 3.8 Mrad irradiation. However, no severe radiation-induced nonuniformity is additionally observed below 1 Mrad. In

order to investigate details of the radiation induced change in response uniformity, we evaluate deviations from the response uniformity measured before irradiation at Y = ±35 mm and ±45 mm: D_{+45}, D_{+35}, D_{-35}, D_{-45}. The deviations were averaged using three data points around each position. The radiation induced nonuniformity is shown in Figure 11 for uniform irradiation and the three cases, A, B, and C, of nonuniform irradiation with 25% dose imbalance. The radiation induced changes in response uniformity are similar to each other except for the case (A). In the case (A), asymmetric nonuniformity is seen at positive and negative sides in Y direction and it is due to nonuniform irradiation. The changes are dependent on radiation doses. The changes for the case (C) seem to be slightly better than the other cases. Figure 12 shows the radiation induced nonuniformity obtained under uniform irradiation condition and nonuniform irradiation ones with 15%, 25%, and 50% dose imbalances in the case (C). The changes are less than ±1% at Y = ±35 mm and ±45 mm below 0.6 Mrad without respect to the dose imbalances. The change seems to increase linearly as doses. The changes become 2-3% in a dose range of 1-7.2 Mrad at Y = ±35 mm and 2-3% in a dose range of 1-3 Mrad and 7-8% in 3-5 Mrad on a waveshifting fiber at Y = ±45 mm. The large changes in response uniformity at Y = ±45 mm would be due to degradation of light transmission in a scintillating tile. Since the data is normalized at the center, the response around the fiber is enhanced. A Monte Carlo study is in progress to understand the radiation induced nonuniformity.

6 Effects of Dose Rate and Gas Environment

Figure 13 shows dose rate dependence of the ^{60}Co-induced radiation damage of SCSN81/Y7 tile/fibers. From the samples G, we selected those samples with total doses in the ranges 0.25-0.45 and 1.10-1.30 Mrad. The data shows that the dose rate dependence is very weak in the range 6-360 krad/h.

Figure 14 shows effects of gas environments on radiation hardness of SCSN81/Y7 tile/fibers. The E_2 samples were irradiated and annealed in air. On the other hand, the E_3 samples were irradiated in nitrogen and annealed in air. The instantaneous dose rate was in the range 1-70 krad/h. The ^{106}Ru- source measurements were made two weeks after the irradiation. The results show that no significant improvement in radiation hardness was obtained in the samples irradiated in nitrogen. We need further studies on the effects of gas environments in exposure at lower dose rates in relation to dose rate dependence.

7 Radiation Hardness

The ^{60}Co exposure for the samples G, K, and L was performed under the irradiation conditions specified in Table 3. Eight pieces of tile/fibers were exposed at the same time in air under these conditions. These conditions were determined in such a way that the tile/fiber samples were irradiated at similar dose rates as expected to the tile/fibers placed at specific depth in the calorimeter test module irradiated with 2.5-GeV electrons[2]. Two reference tile/fibers were

Table 3: Irradiation conditions used in the radiation hardness test of scintillating tile/fibers with ^{60}Co. These conditions were determined in such a way that the tile/fiber samples were irradiated at similar dose rates as expected to the tile/fibers placed at specific layer number in the calorimeter test module irradiated with 2.5-GeV electrons. These samples were exposed in air. Dose Rate denotes the instantaneous dose rate.

Condition#	Layer#	Source (kCi)	Distance (cm)	Dose Rate (krad/h)
1	4	110	37.5	360
2	3,5	110	38.5	340
3	2,7	110	48	227
4	9	110	65	123
5	1	5.9	17.5	82
6	12	5.9	24	46
7	16	5.9	50	12
8	18	5.9	70	6

evaluated as well without any irradiations so as to investigate systematics in measurements.

First, we investigated the radiation damage of the SCSN81/Y7 tile/fibers in the K group under the following two conditions: (1) Keeping continuous irradiation under the condition specified in Table 3 for 16.5 hours. (2) Interrupting the irradiation right after every 5.5-hour irradiation followed by 18.5-hour intermission, and continueing it for 3 days. Under the condition (2), the average dose rate is reduced to about 30%, although the instantaneous dose rate is the same as in the case (1). The ^{106}Ru-source measurements were made one week after the irradiation. The results are shown in Figure 15. No difference was observed between the continuous and discontinuous irradiations. The permanent radiation damage measured after completing of annealing seems to be insensitive to whether the irradiation was interrupted.

Next, we compare the ^{60}Co exposure results with the radiation damage induced by 2.5-GeV electron showers. Figure 16 shows radiation hardness of the samples E_1, E_2, and C, which were irradiated with 2.5-GeV electron showers at KEK. As described in Section 3, radiation hardness of each sample was defined by taking a ratio of the effective light yield measured after irradiation to that measured before. The effective light yield was evaluated by measuring ^{106}Ru-induced currents. There are nine tile/fibers in the C samples selected after dismounting the calorimeter test module C which was exposed up to 5 Mrad at the shower maximum. The E_1 and E_2 tile/fibers were inserted at typical depths along the lead absorber stack as specified in Table 3. From Figures 15 and 16, we find that the damage induced by 2.5-GeV electron showers is in agreement with the ^{60}Co-induced damage. It should also be noted that these results are in agreement with those obtained by measuring the pulse height distribution of 2.0-GeV electrons for the specific tile/fibers placed in the calorimeter test module A and B. These modules were exposed up to 0.8 and 0.4 Mrad at the shower maximum. Combining these results with those in

Figure 4, we find that our results on the radiation hardness are independent of how to evaluate it by ^{106}Ru-induced current, penetrating β rays, or high energy electron beam.

Finally we compare the radiation hardness of various tile/fiber combinations. Figure 17 shows the radiation hardness of five combinations of scintillating tile/fibers: SCSN81/Y7, SCSN81/BCF91A, SCSN38/Y7, SCSN81Y7/O2, and 3HF/O2. These samples L were exposed to ^{60}Co γ-rays under the irradiation conditions in Table 3 and the radiation hardness was evaluated by measuring ^{106}Ru-induced currents. The number in parentheses is a relative light yield of each tile/fiber sample measured by using a Hamamatsu R580 photomultiplier tube. Since the R580 is a blue-sensitive photomultiplier, the relative light yields of SCSN81Y7/O2 and 3HF/O2 using orange waveshifting fibers are lower than the others using green waveshifting fibers. However, the radiation hardness of these tile/fibers using a green tile with an orange fiber is better than those using a blue tile with a green fiber. Especially the 3HF/O2 is significantly radiation-resistant. The radiation hardness of the 3HF/O2 is 50% at 7 Mrad, while the SCSN81/Y7 is damaged down to 20%. Comparison of the SCSN81/Y7 and SCSN81/BCF91A shows that no significant difference is observed in the relative light yield and that the radiation hardness is quite similar up to a few Mrad.

The data shown in Figure 17 are preliminary. They were taken with a new ^{106}Ru-source scanner, which was not fully checked out. The data points with low light yield may suffer from errors of ± 0.05 in the light yield ratio. We plan a final measurement in the near future and will report it in a revised version of this note.

8 Conclusions

We have investigated the ^{60}Co-induced damage of scintillating tile/fibers. The main results are as follows. (1) At a high dose rate of 264 krad/h, annealing of the radiation damage is seen with a time constant of 1-4 hours, while a drastic change is not seen at a lower dose rate of 18 krad/h. (2) Additional radiation-induced nonuniformity is observed above 1 Mrad. The changes become 2-3% in a dose range of 1-7.2 Mrad at Y = ± 35 mm and 2-3% in a dose range of 1-3 Mrad and 7-8% in 3-5 Mrad on a waveshifting fiber at Y = ± 45 mm. However, the changes are less than ± 1% below 0.6 Mrad even if the dose imbalance is as much as 50% in a tile. (3) Dose rate dependence of the radiation damage is very weak in the range 6-360 krad/h. (4) No significant improvement in radiation hardness was obtained in the samples irradiated in nitrogen and annealed in air. (5) The damage induced by 2.5-GeV electron showers is in agreement with the ^{60}Co-induced damage. Our results on the radiation hardness are independent of how to evaluate it, ^{106}Ru-induced current, penetrating β rays, or high energy electron beam. (6) The radiation hardness of the tile/fibers using a green tile with an orange fiber is better than those using a blue tile with a green fiber, although the relative light yield of the latter is better than the former due to less sensitivity of the photomultiplier to orange lights. Especially the 3HF/O2 is significantly radiation-resistant. The radiation hardness of 3HF/O2 is 50% at 7 Mrad, while SCSN81/Y7 is damaged down to 20%. (7) Comparison of the SCSN81/Y7 and SCSN81/BCF91A shows that

no significant difference is observed in the relative light yield and that the radiation hardness is quite similar up to a few Mrad. Above 5 Mrad, the SCSN81/BCF91A seems to be slightly more resistant to radiation, but the difference is marginal.

As shown in Reference [2], the radiation hardness of the scintillating tile/fiber calorimeters using SCSN81/Y7 is good enough for use in the barrel region for 70 years or longer at the design luminosity of 10^{33} $cm^{-2}sec^{-1}$ before 1% degradation in energy resolution takes place. The combination SCSN81/BCF91A replacing Y7 fiber by BCF91A fiber has been shown to have essentially the same characteristics as far as the radiation hardness and the light yield are concerned. The combination 3HF/O2 or SCSN81Y7/O2 needs more light yields for use in the barrel calorimeter. In the endcap region, much improvement in radiation hardness than SCSN81/Y7 combination is required. The 3HF/O2 combination is a good candidate for the endcap calorimeter. Further developments of orange and red sensitive photomultiplier tubes would improve light yields.

Acknowledgement

We would like to thank H. Nagayama and T. Ohkubo of Japan Atomic Energy Research Institute at Tokai for performing the ^{60}Co irradiation to the scintillator samples. We would also like to thank to M. Sunaga of Japan Atomic Energy Research Institute at Takasaki for performing the calibration of the dosimeters.

References

[1] L. Hu *et al.*, "Radiation damage of tile/fiber scintillator modules for the SDC calorimeter", Solenoidal Detector Collaboration Note SDC-91-00119 (1991).

[2] S. Funaki *et al.*, "Beam test of radiation hardness of a scintillating tile/fiber calorimeter.", Solenoidal Detector Collaboration Note SDC-91-00085 (1991), (submitted to Nucl. Instr. and Meth. A).

[3] P. Bonamy *et al.*, "Radiation damage in tile-fiber calorimeter modules.", Solenoidal Detector Collaboration Note SDC-91-00126 (1991).

[4] "Proceedings of the workshop on radiation hardness of plastic scintillator", ed. by K. F. Johnson, Tallahassee, Florida, March 19-21, 1990.

[5] See for example, R. Clough, "Radiation damage to polymers", in "Workshop on scintillating fiber detector development for the SSC", (1988) Fermilab.

[6] D. E. Groom, "Proc. of the 1988 Summer Study on High Energy Physics in the 1990's", ed. by F. J. Gilman and S. Jensen, Snowmass CO, July 1988 (1989);

"Report for the Task Force on Radiation Levels in the SSC Interaction Regions," ed. by D. E. Groom, SSC Central Design Group Report SSC-SR-1033 (June 1988).

[7] T. Iinuma *et al.*, "Effects of Gas Atmosphere on ^{60}Co-induced radiation damage of scintillating fibers", CDF Note CDF-1068 (1989).

[8] Type FTR-125, Fuji photo film Co. Ltd., Tokyo 106, Japan.

[9] K. C. Humpherys and A. D. Kantz, Radiat. Phys. Chem. 9 (1977) 737; Far West Technologies, Goleta, Ca.

[10] M. Atac, W. Foster, and M. Lundin, "A Simple Method for Fusing Plastic Fibers", Fermilab Note FN-537 (1990).

[11] The heat-welding splicer was designed and produced by Kuraray.

[12] K. T. Gillen and R. L. Clough, "Quantitative confirmation of simple theoretical models for diffusion-limited oxidation.", in "Radiation Effects on Polymers", ed. by R. L. Clough and S. W. Shalaby, ACS Symposium Series 475, August 26-31, 1990.

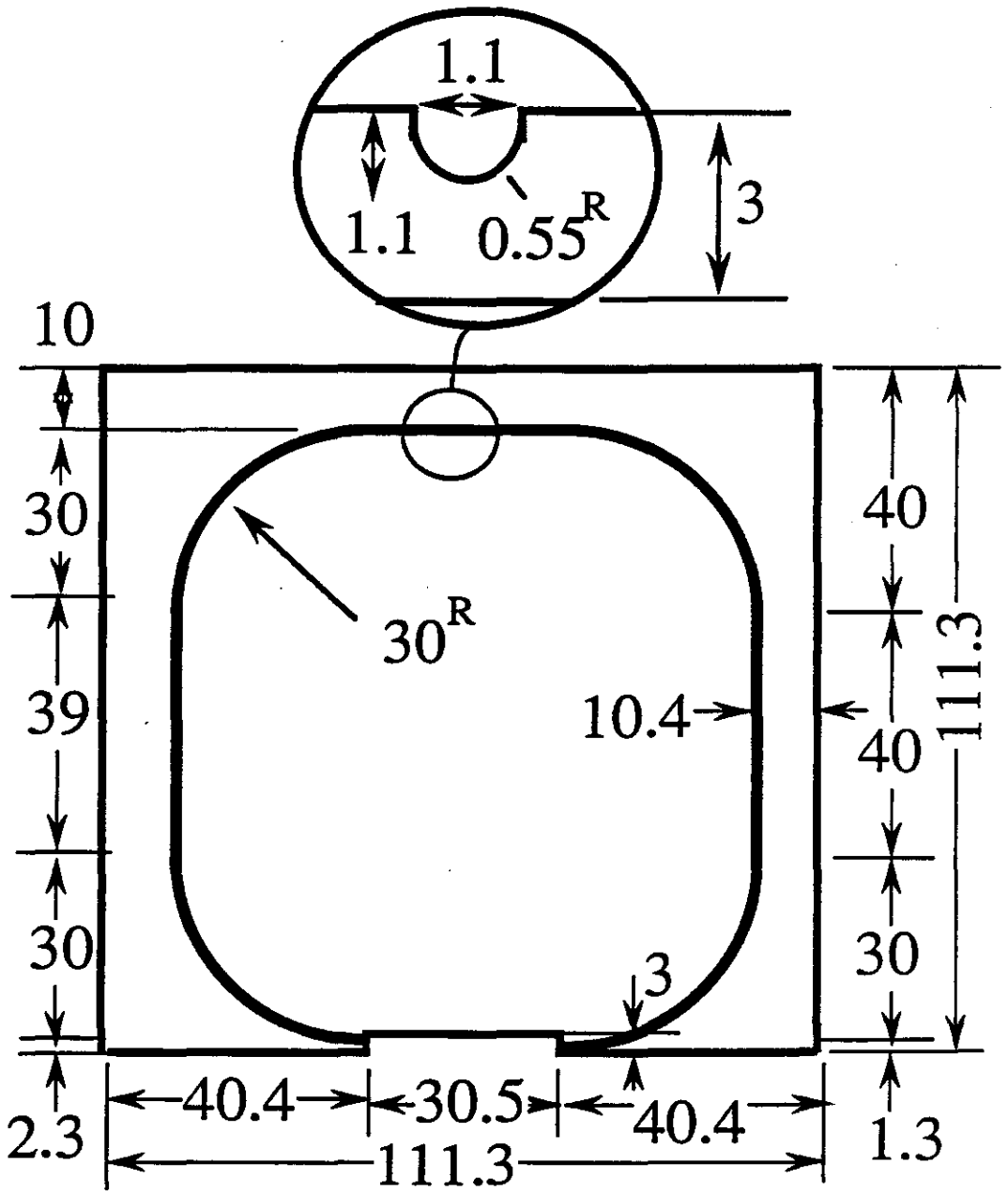

Figure 1: A schematic diagram of scintillating tile. (Unit is in mm.)

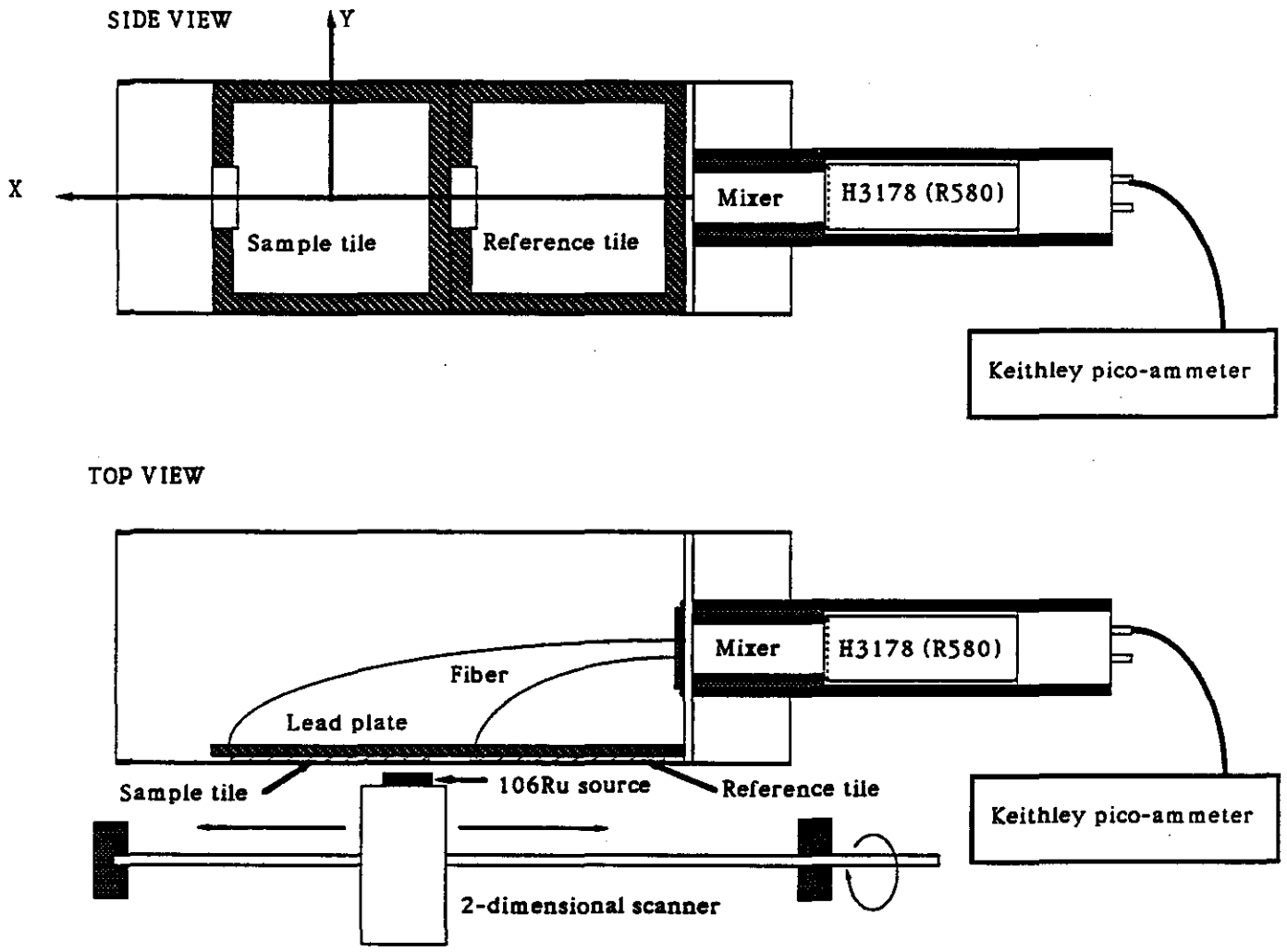

Figure 2: A schematic view of 2-dimensional scanner in ^{106}Ru-induced current measurements.

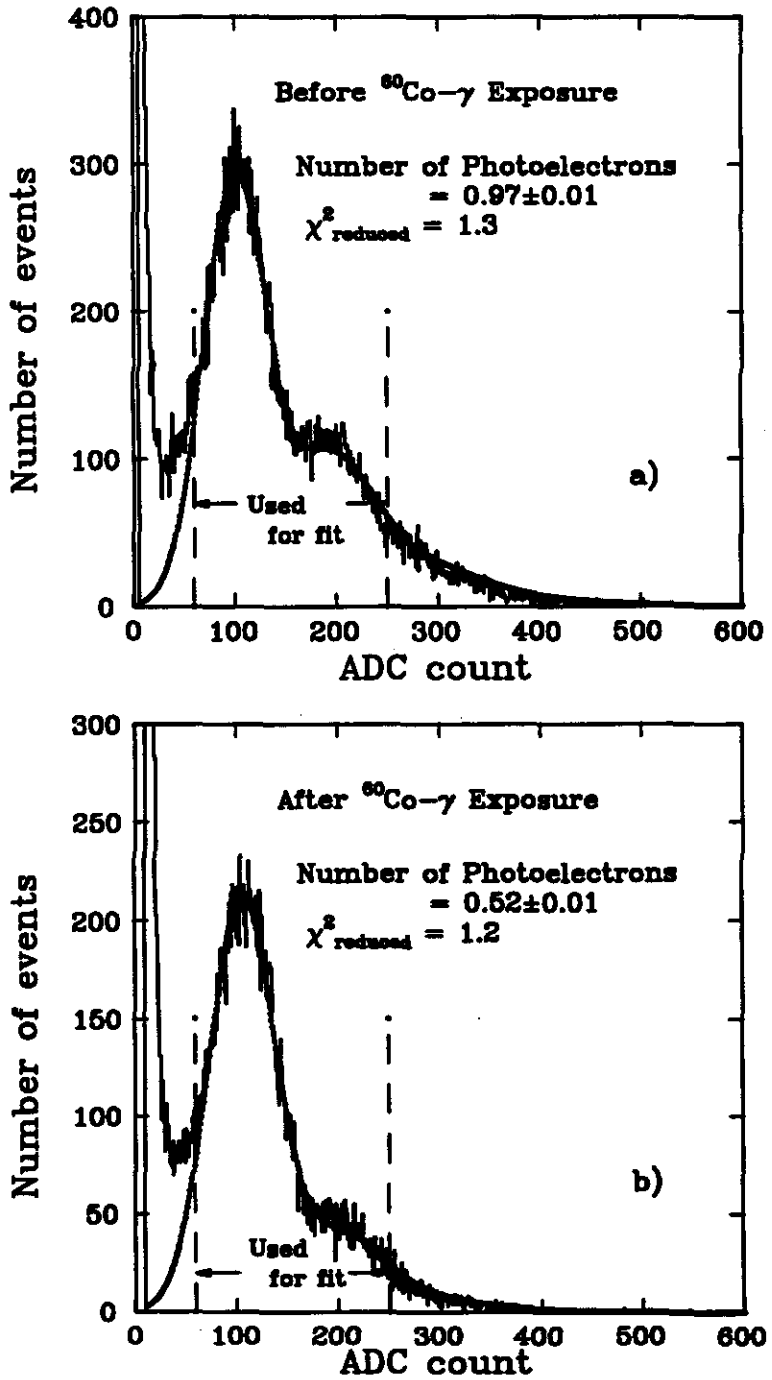

Figure 3: Pulse height distributions measured (a) before and (b) after ^{60}Co irradiations for the sample I4. The number of photoelectrons were measured by fitting the pulse height distribution to a convolution of Poisson and Gaussian distributions. Only data within dashed lines was fitted in evaluation of the number of photoelectrons.

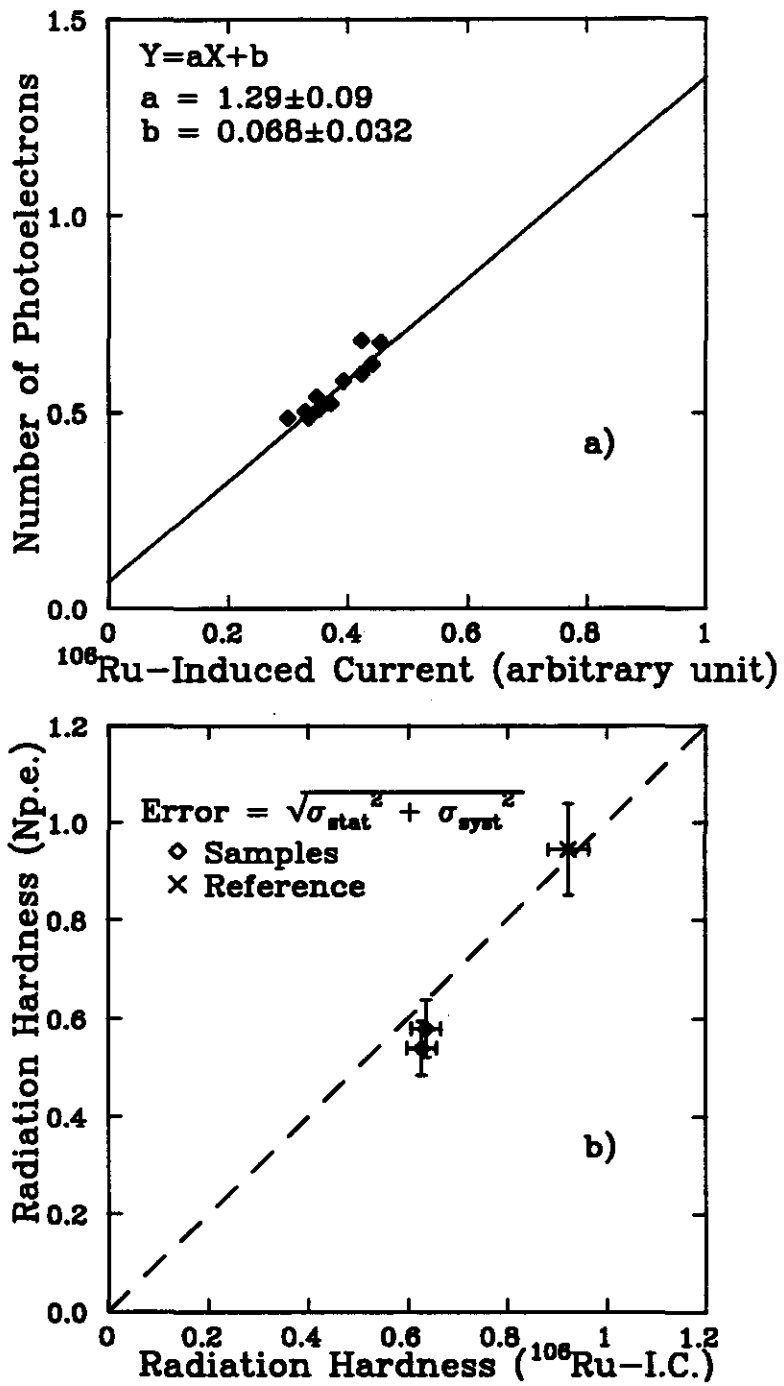

Figure 4: (a) Correlation between ^{106}Ru-induced currents and the number of photoelectrons measured with ^{90}Sr. (b) Comparison of radiation damage evaluated by measuring the number of photoelectrons with penetrating electrons from ^{90}Sr β decay and by measuring the ^{106}Ru-induced currents.

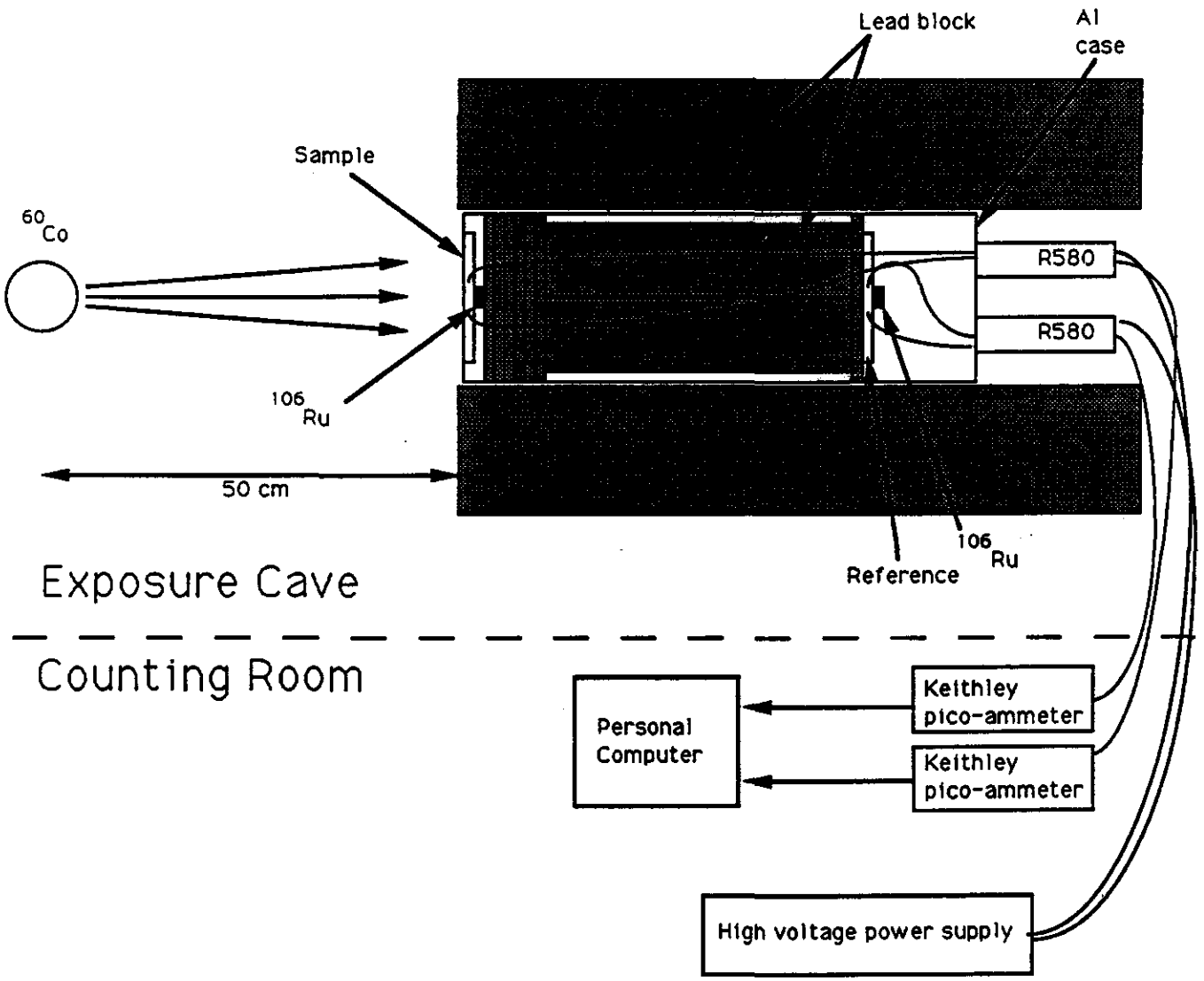

Figure 5: A schematic view of the setup used for measurements of annealing effects of radiation damage for scintillating tile/fibers.

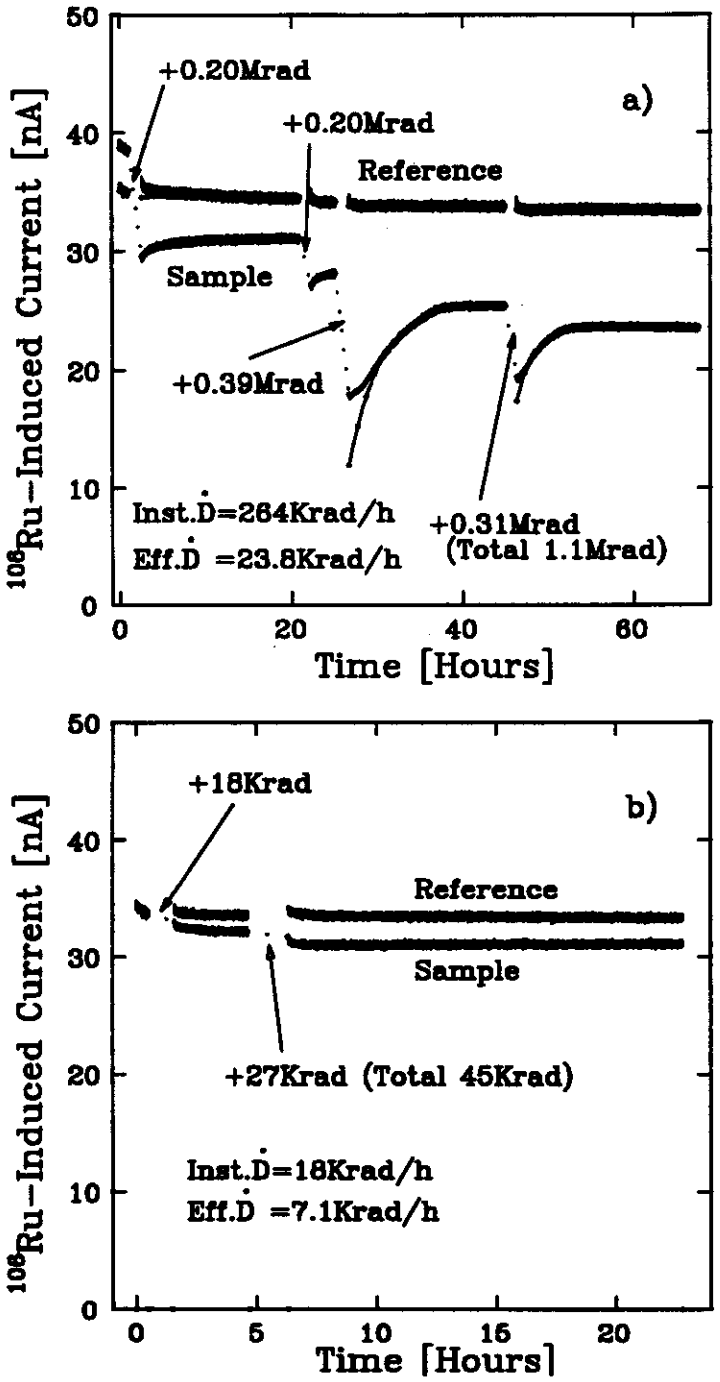

Figure 6: A history of radiation damage of the scintillating tile/fiber samples (a) H1 and (b) H2.

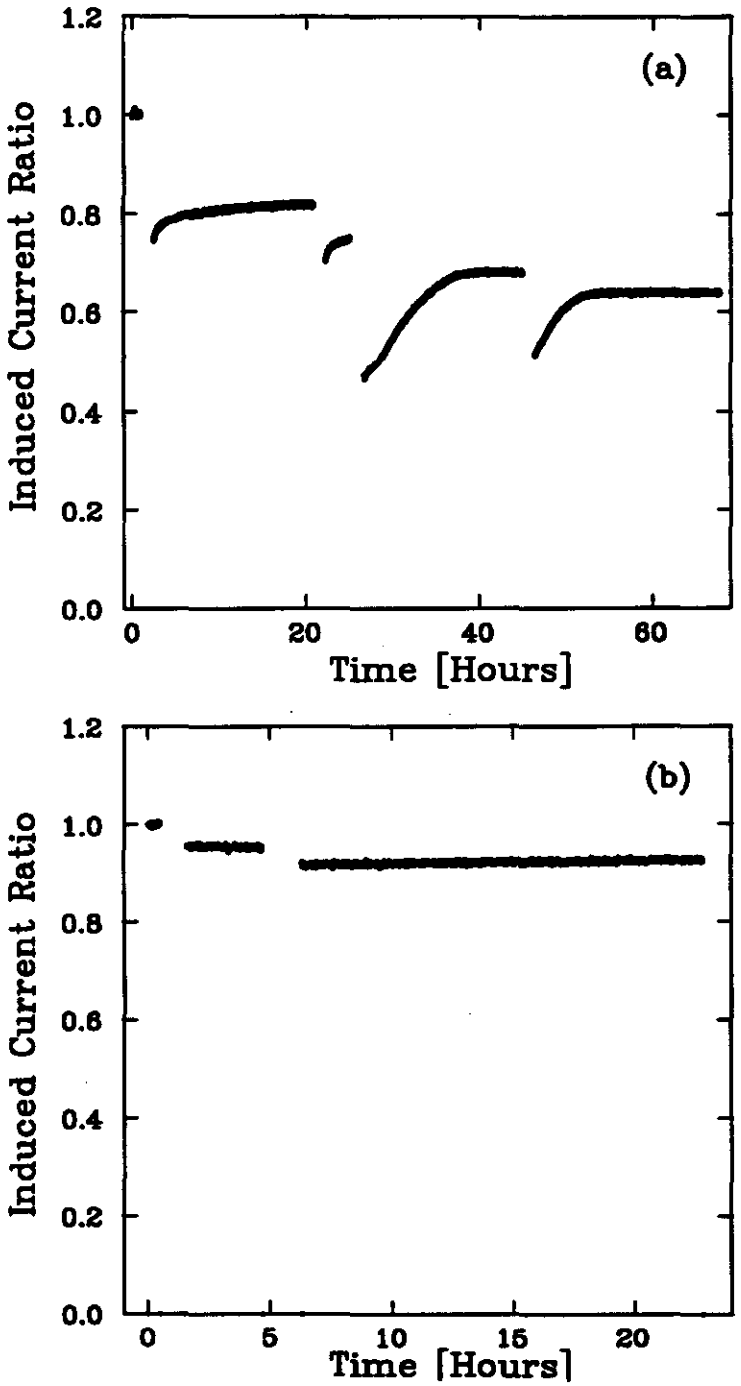

Figure 7: A history of radiation damage of the scintillating tile/fiber samples (a) H1 and (b) H2. In order to cancel considerable part of variations originating from common sources, we took a ratio of the sample current to the reference current. The ratio is normalized at the start time of the current measurement.

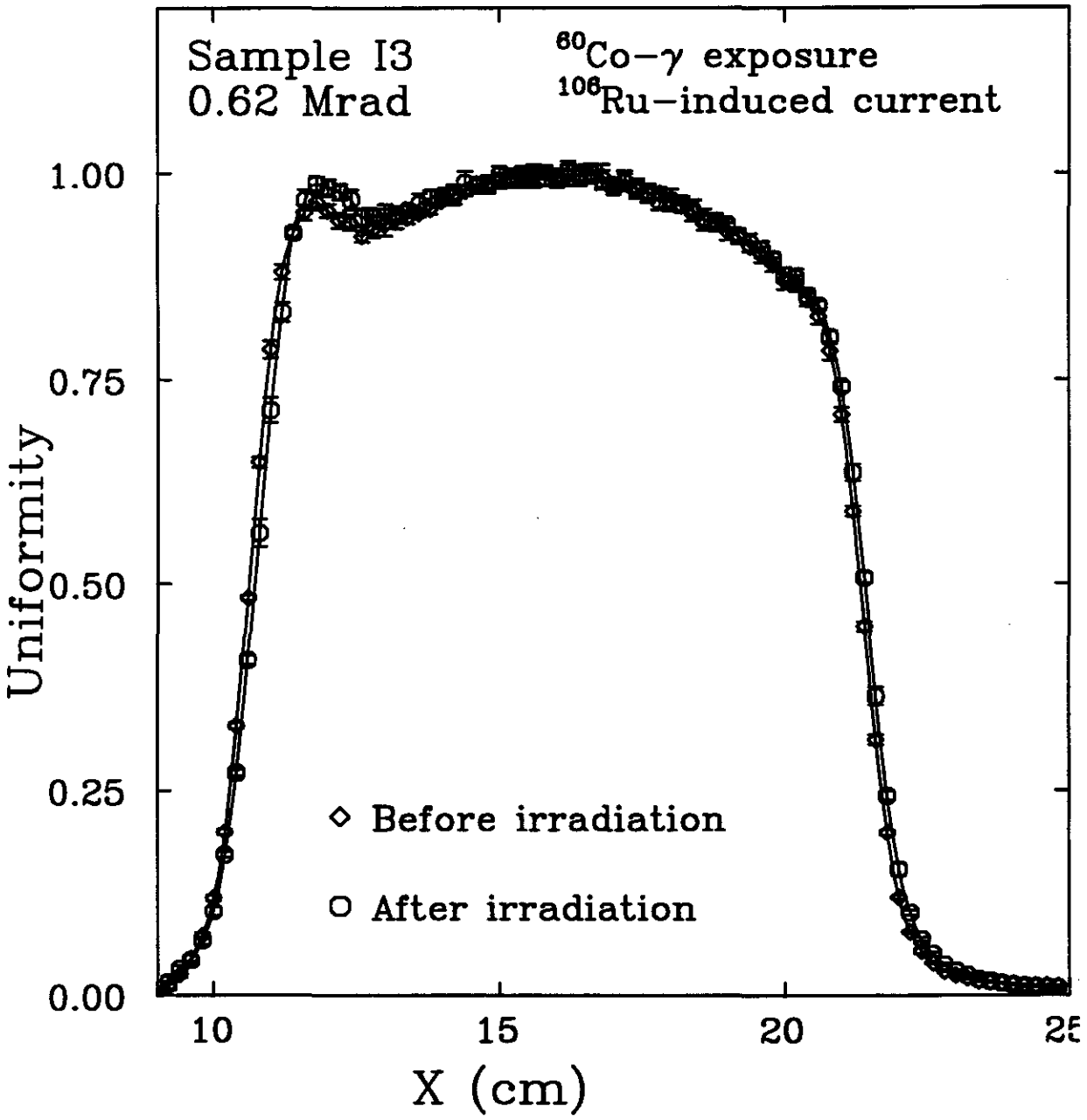

Figure 8: The sample I3 was mapped by measuring ^{106}Ru-induced currents before and after ^{60}Co exposures and their response uniformities were compared. No significant difference was observed.

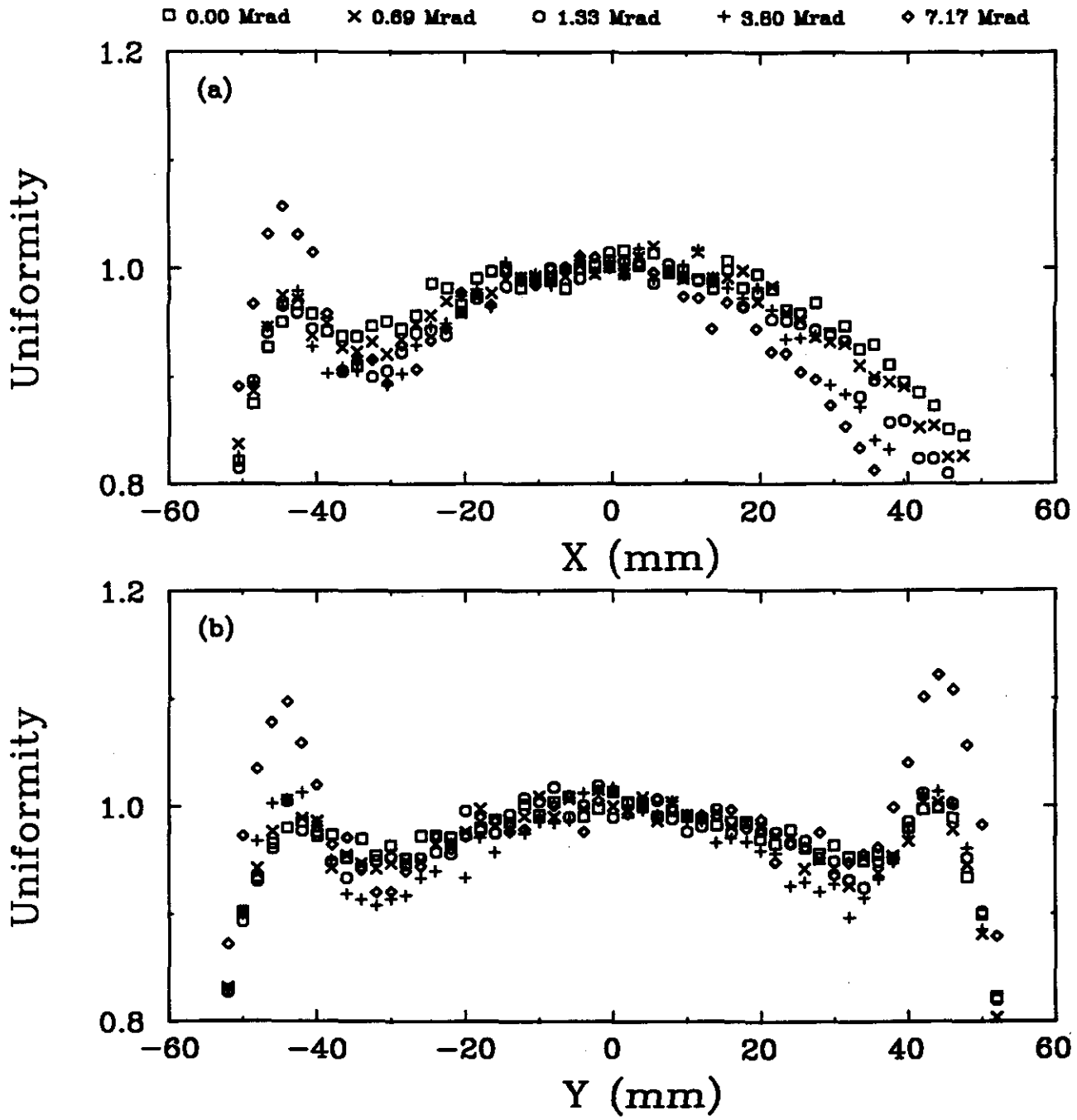

Figure 9: The response uniformity obtained before (square) and after uniform irradiation of 0.69 Mrad (cross), 1.33 Mrad (circle), 3.80 Mrad (plus), and 7.17 Mrad (diamond). The scanning was performed to the direction (a) parallel to the symmetrical axis of the tile/fiber at the tile/fiber center and to the direction (b) perpendicular to the symmetrical axis. The waveshifting fiber is placed at X = −45 mm in (a) and at Y = ±45 mm in (b).

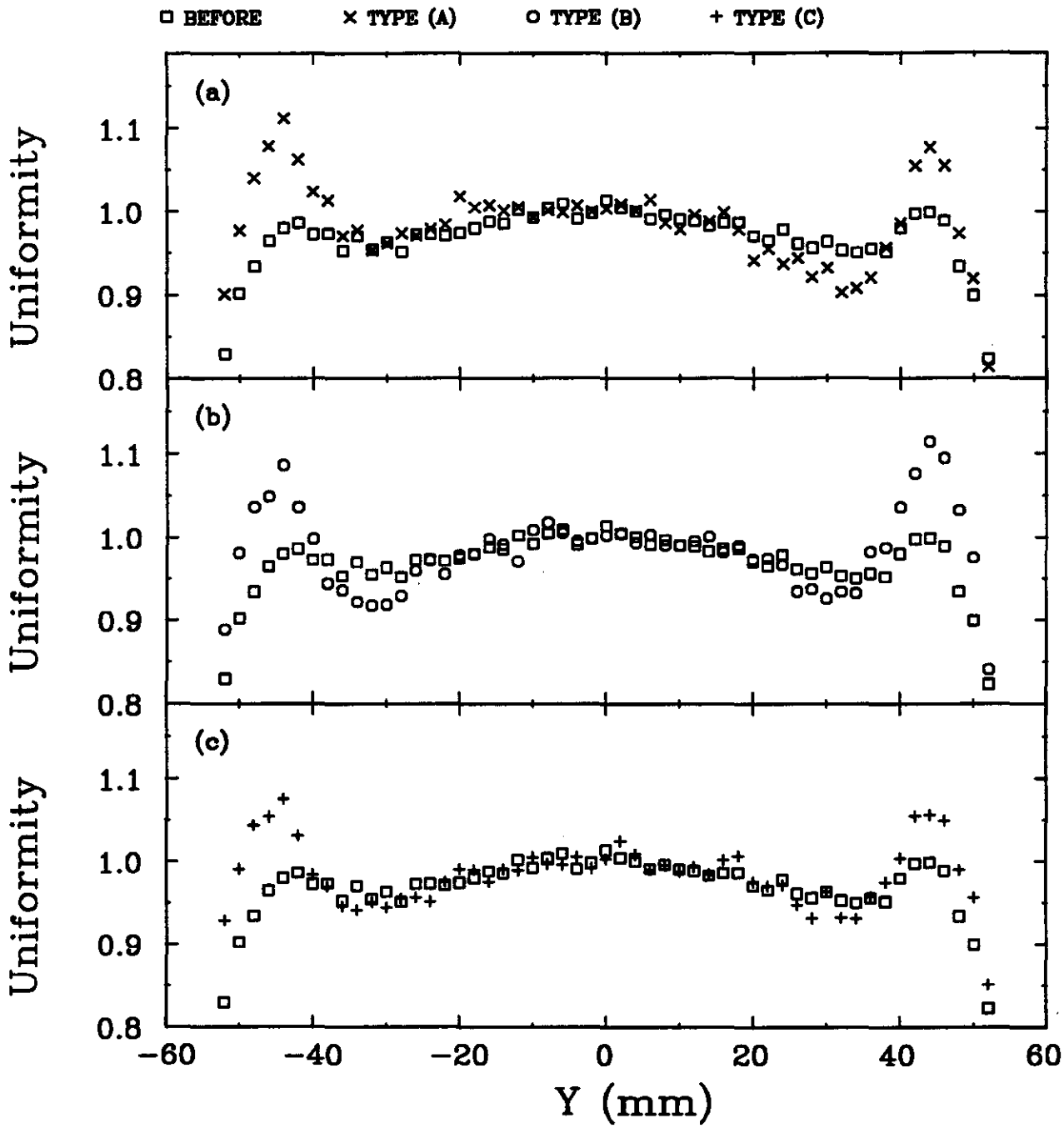

Figure 10: The response uniformity obtained before (square) and after 4.2 Mrad irradiation with 25% dose imbalance at peak-to-peak. The scanning was performed to the direction perpendicular to the symmetrical axis of the tile/fiber at the tile center. The top, middle, and bottom plots correspond to three cases, (A), (B), and (C), described in the text.

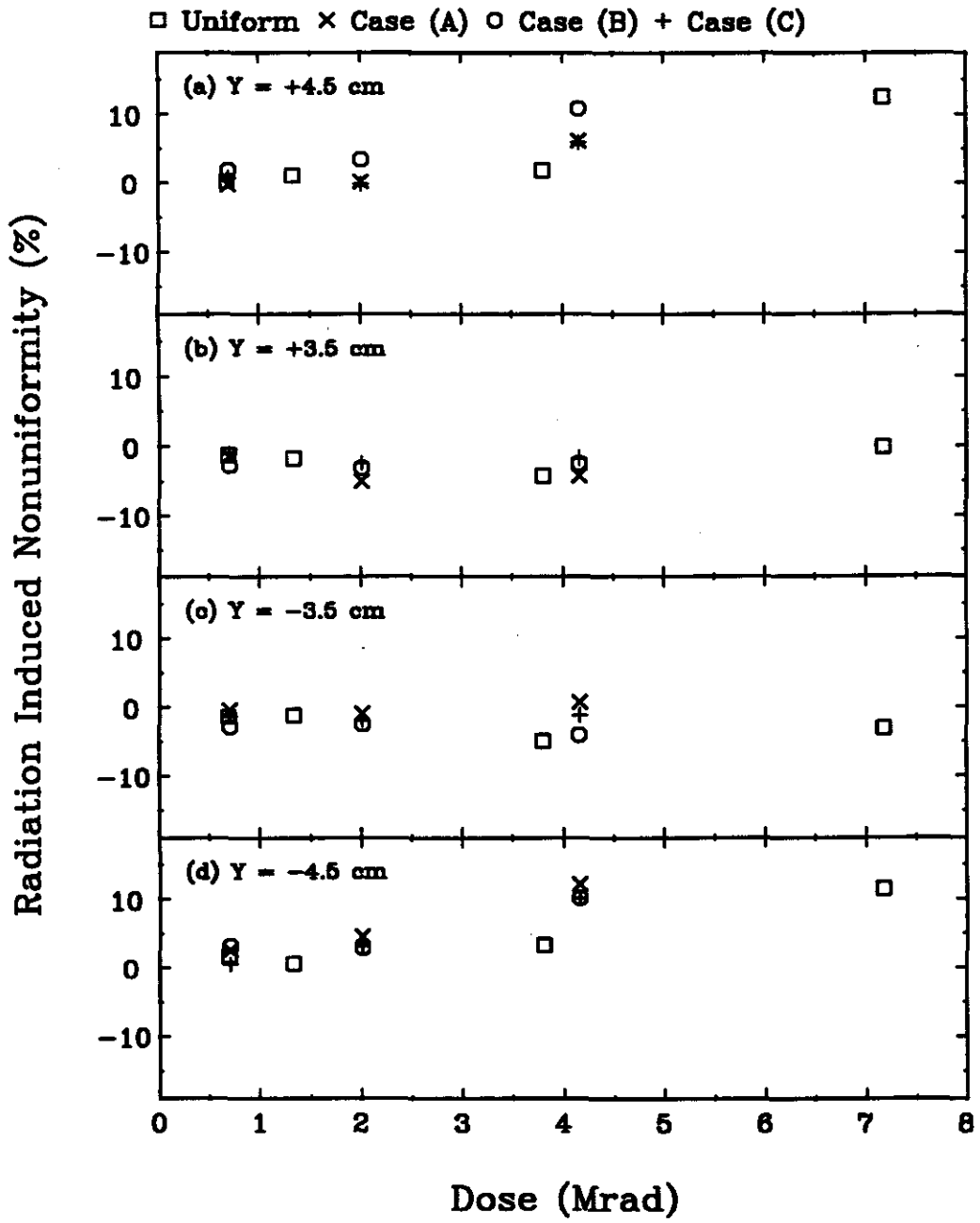

Figure 11: The radiation-induced change in response uniformity of SCSN81/Y7 obtained at Y = ±35 and ±45 mm with uniform irradiation (square) and with 25% dose imbalance at peak-to-peak for the cases (A) (cross), (B) (circle), and (C) (plus).

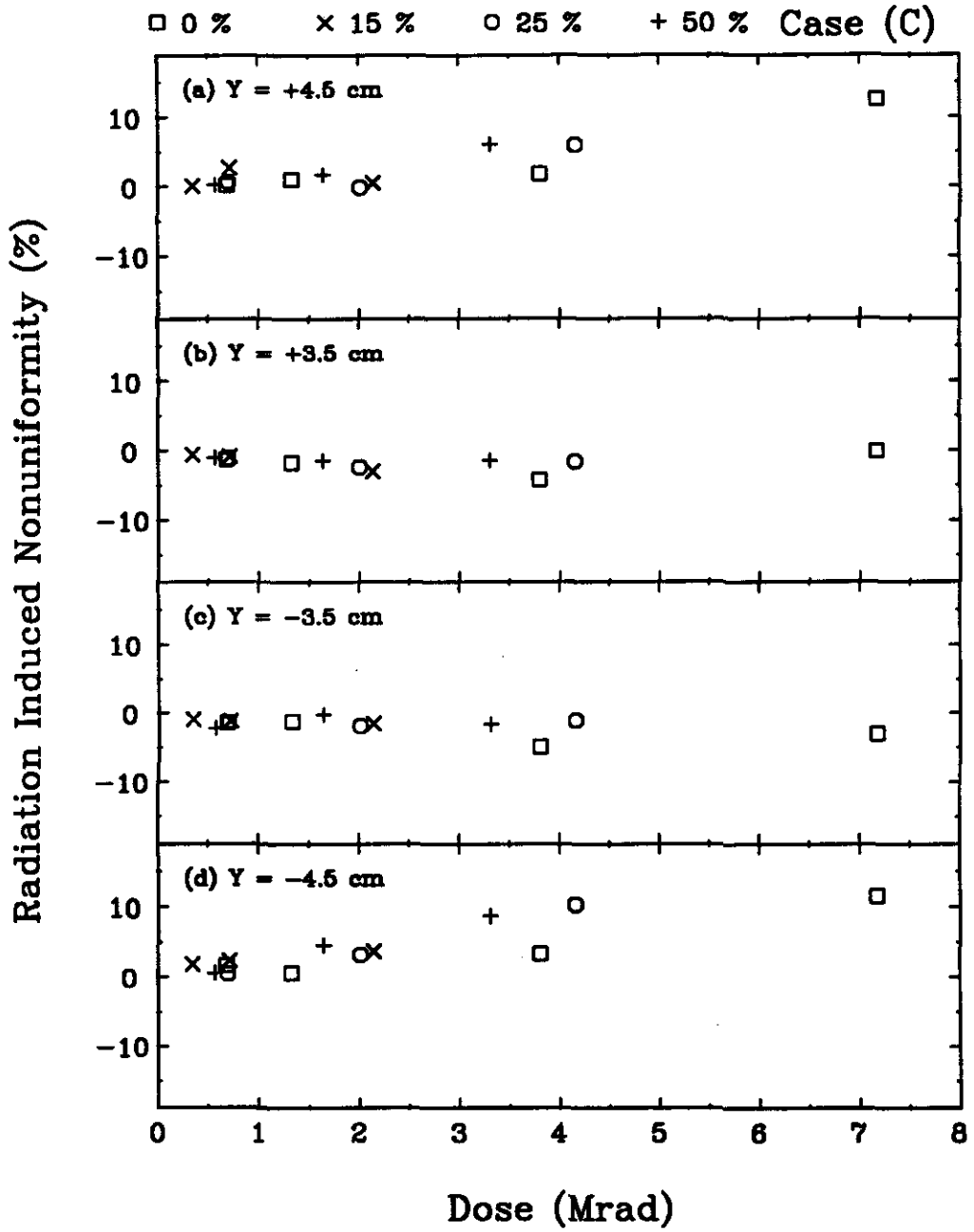

Figure 12: The radiation induced change in response uniformity of SCSN81/Y7 obtained at Y = ±35 and ±45 mm under uniform irradiation condition (square) and under nonuniform irradiation conditions of 15% (cross), 25% (circle), and 50% (plus) dose imbalances at peak-to-peak for the case (C).

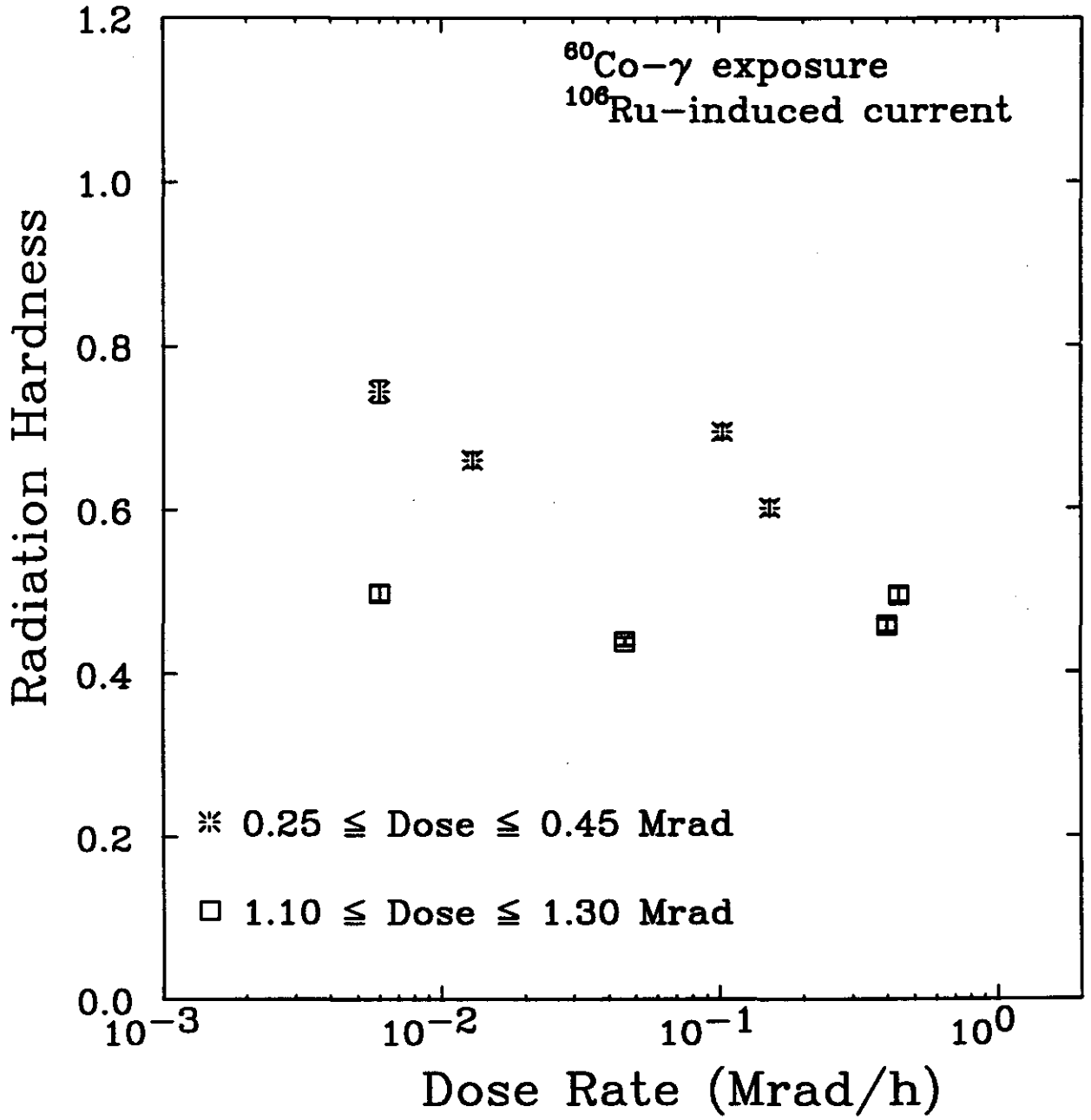

Figure 13: Dose rate dependence of ^{60}Co-induced radiation damage of SCSN81/Y7 tile/fibers.

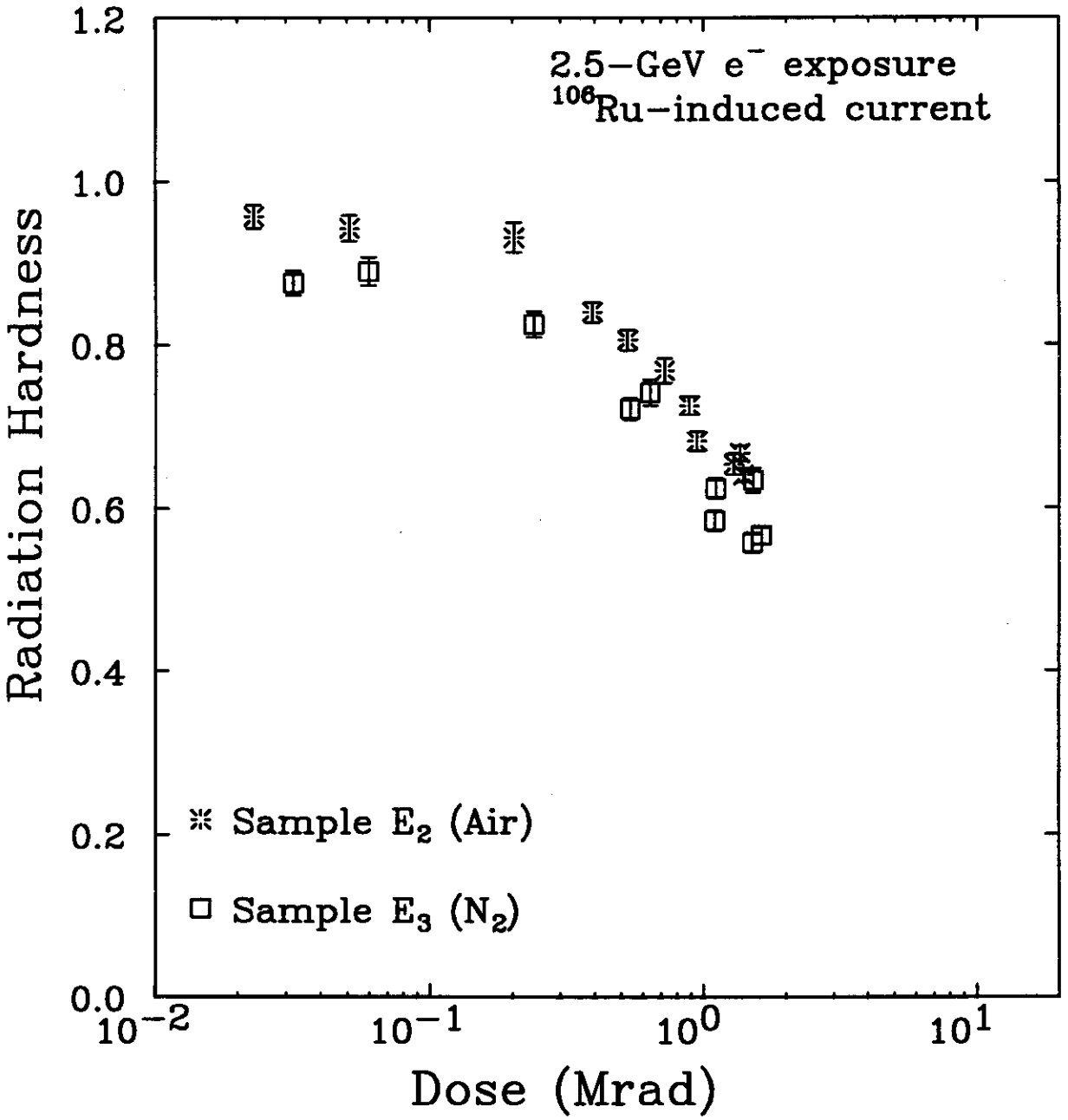

Figure 14: Effects of gas environment on radiation hardness of SCSN81/Y7 tile/fibers. The samples E_2 and E_3 were irradiated in air and nitrogen gases, respectively. The ^{106}Ru- source measurements were made after two weeks from the irradiation.

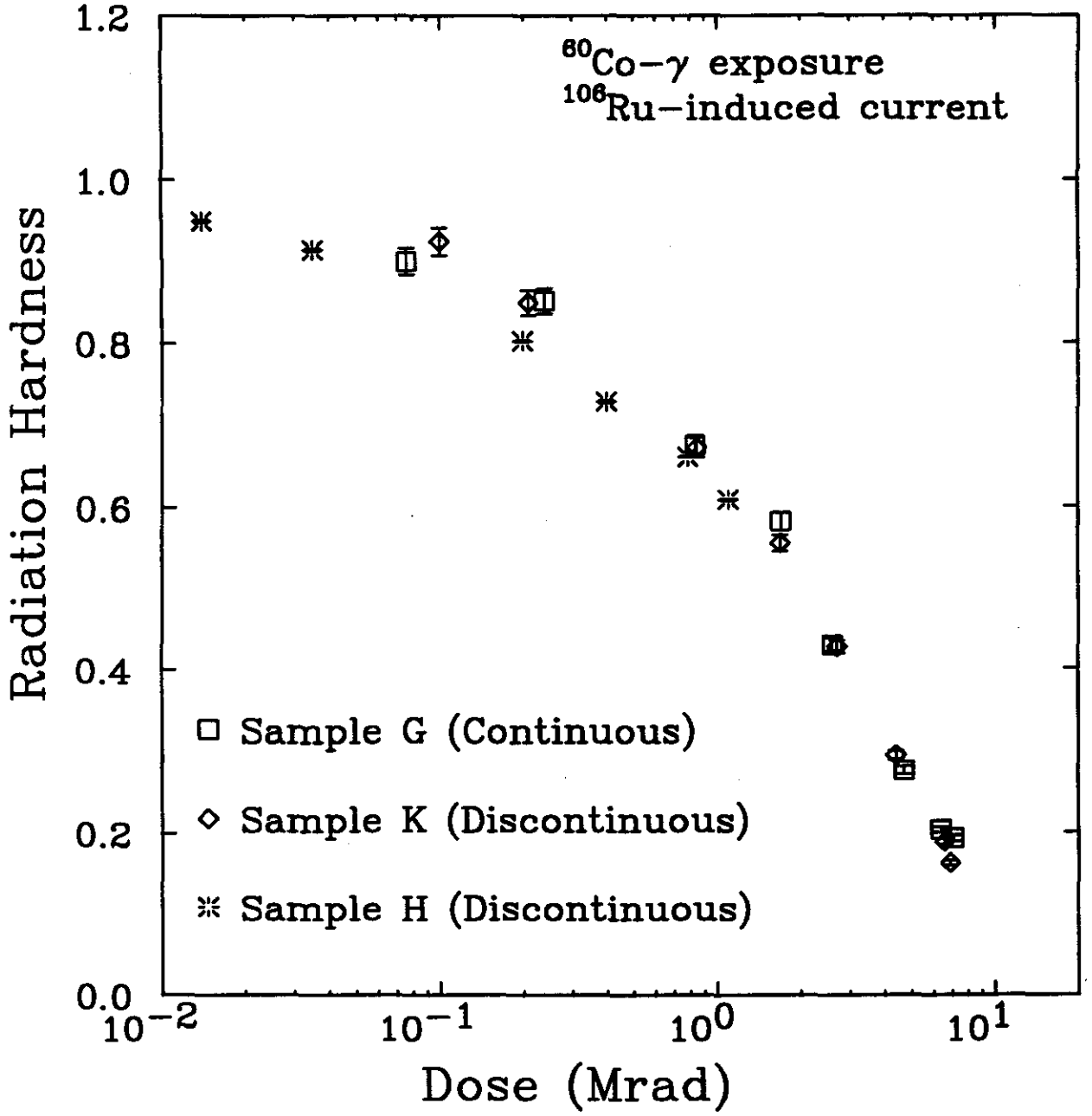

Figure 15: Radiation hardness of the continuously-irradiated sample G and the discontinuously-irradiated samples K and H.

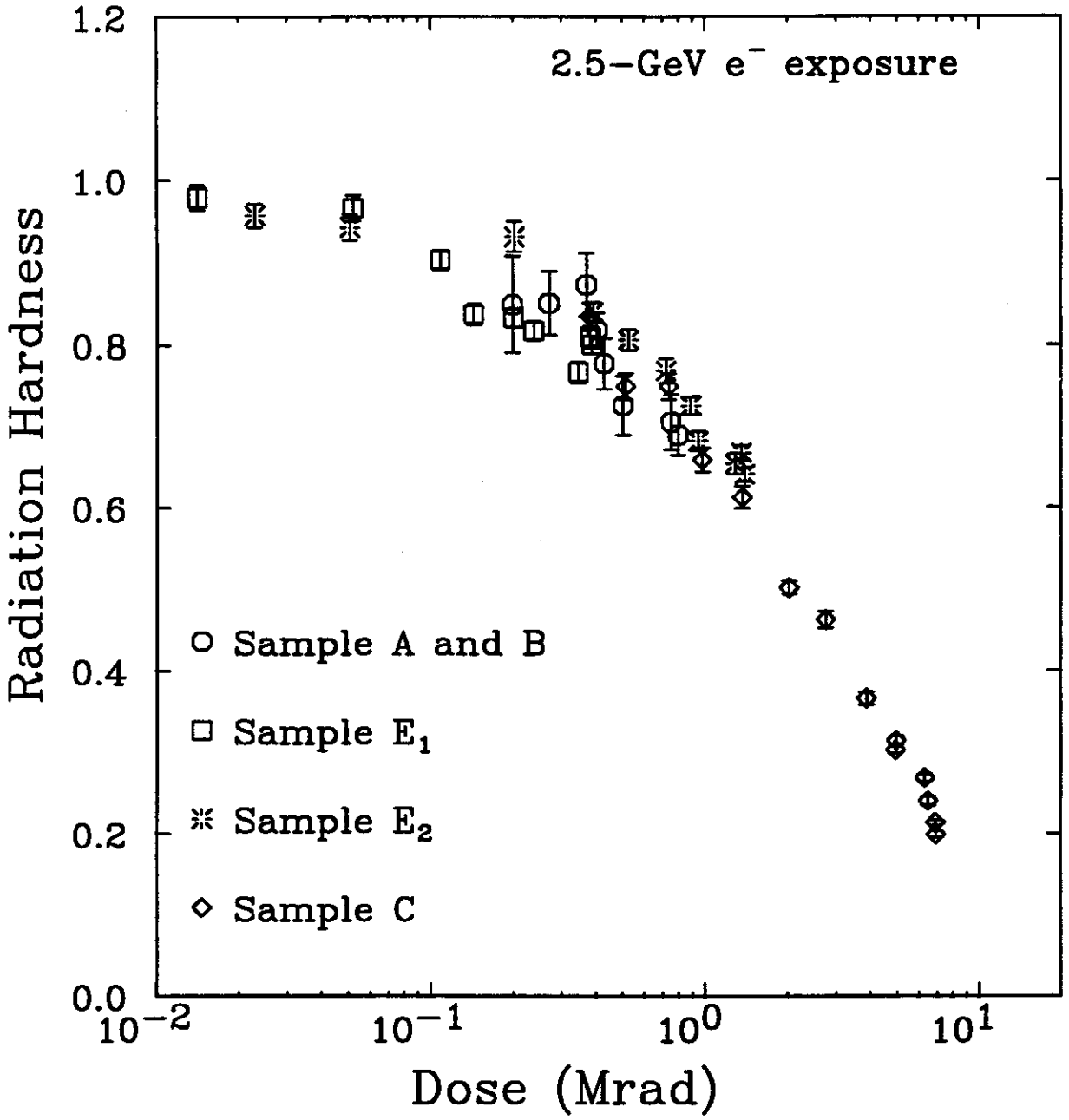

Figure 16: Comparison of the radiation hardness of the samples A, B, E_1, E_2, and C. Although all the samples were exposed to 2.5-GeV electron showers, the evaluation of the radiation hardness was made by measuring the pulse height distribution of 2.0-GeV electrons for A and B, and the ^{106}Ru-induced currents for E_1, E_2, and C.

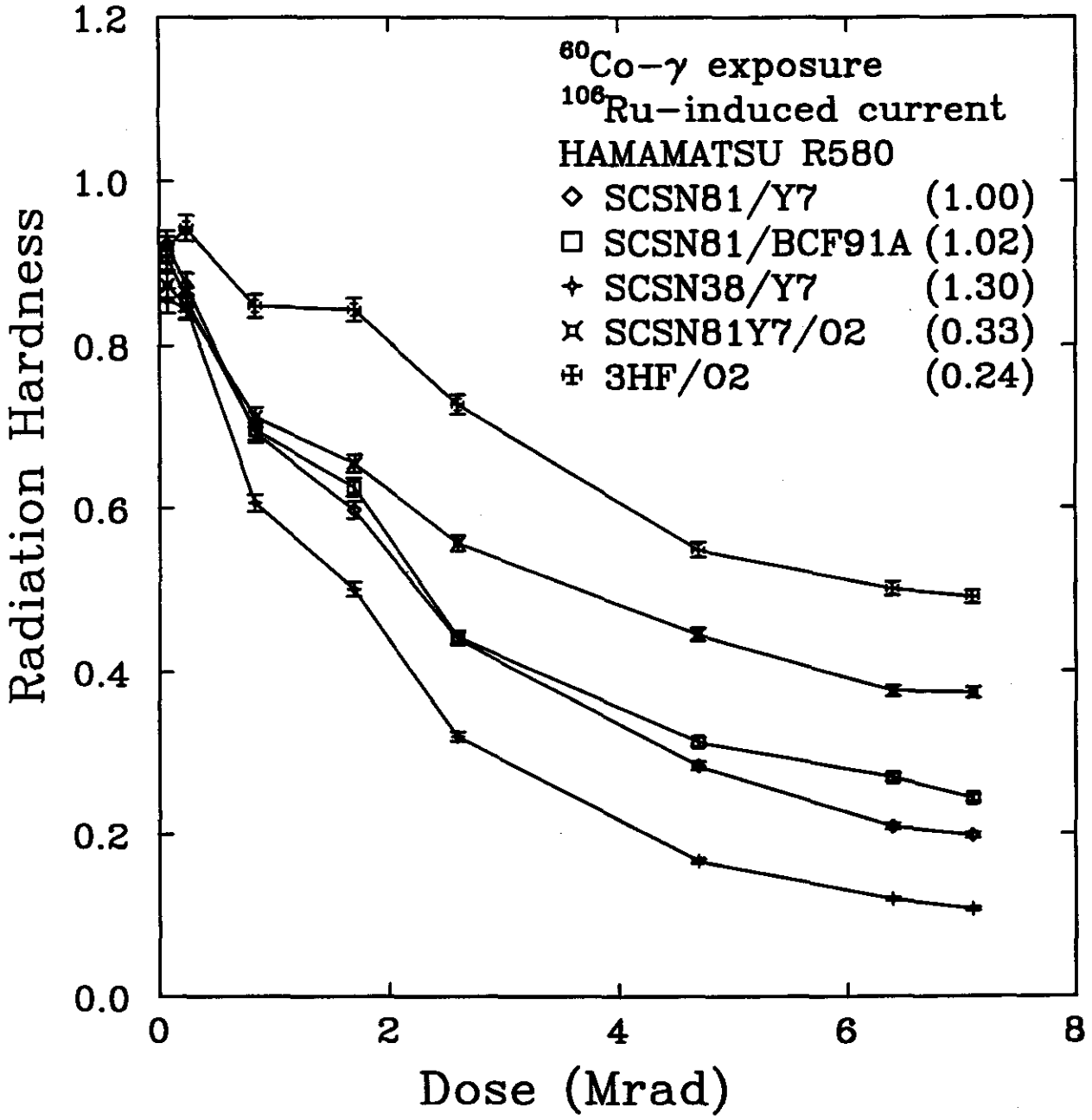

Figure 17: Comparison of radiation hardness of scintillating tiles with waveshifting fibers; SCSN81/Y7, SCSN81/BCF91A, SCSN38/Y7, SCSN81Y7/O2, and 3HF/O2. These samples were exposed to ^{60}Co γ-rays and evaluated by measuring ^{106}Ru-induced currents. The number in parentheses indicates a relative light yield of each tile/fiber sample measured by using Hamamatsu R580. Data is joined together by a solid curve for convenience.